White Rose Research Online

eprints@whiterose.ac.uk
https://eprints.whiterose.ac.uk
Universities of Leeds, Sheffield and York

Deposited via The University of Sheffield.

White Rose Research Online URL for this paper:
https://eprints.whiterose.ac.uk/id/eprint/129004/

Version: Accepted Version

Article:
Walkley, B., Rees, G., San Nicolas, R. et al. (2018) New Structural Model of Hydrous Sodium Aluminosilicate Gels and the Role of Charge-Balancing Extra-Framework Al. The Journal of Physical Chemistry C, 122 (10). pp. 5673-5685. ISSN: 1932-7447

https://doi.org/10.1021/acs.jpcc.8b00259

Reuse
Items deposited in White Rose Research Online are protected by copyright, with all rights reserved unless indicated otherwise. They may be downloaded and/or printed for private study, or other acts as permitted by national copyright laws. The publisher or other rights holders may allow further reproduction and re-use of the full text version. This is indicated by the licence information on the White Rose Research Online record for the item.

Takedown
If you consider content in White Rose Research Online to be in breach of UK law, please notify us by emailing eprints@whiterose.ac.uk including the URL of the record and the reason for the withdrawal request.

A New Structural Model of Sodium Aluminosilicate Gels and the Role of Charge Balancing Extra-Framework Al

Brant Walkley[1, 2] *, Gregory J. Rees[3], Rackel San Nicolas[4], Jannie S.J. van Deventer[2, 5], John V. Hanna[3], John L. Provis[1] *

[1] *Department of Materials Science and Engineering, The University of Sheffield, Sheffield S1 3JD, United Kingdom*

[2] *Department of Chemical and Biomolecular Engineering, The University of Melbourne, Victoria 3010, Australia*

[3] *Department of Physics, The University of Warwick, Coventry CV4 7AL, United Kingdom*

[4] *Department of Infrastructure Engineering, The University of Melbourne, Victoria 3010, Australia*

[5] *Zeobond Pty Ltd, P.O. Box 23450, Docklands, Victoria 8012, Australia*

* Corresponding authors. Email: b.walkley@sheffield.ac.uk and j.provis@sheffield.ac.uk

Abstract

A new structural model of hydrous alkali aluminosilicate gel (N-A-S-H) frameworks is proposed, in which charge balancing extra-framework Al species are observed in N-A-S-H gels for the first time. This model describes the key nanostructural features of these gels, identified through application of ^{17}O, ^{23}Na and ^{27}Al triple quantum magic angle spinning (3QMAS) solid state nuclear magnetic resonance (NMR) spectroscopy to synthetic ^{17}O-enriched gels of differing Si/Al ratios. The alkali aluminosilicate gel is predominantly comprised of $Q^4(4Al)$, $Q^4(3Al)$, $Q^4(2Al)$ and $Q^4(1Al)$ Si units charge-balanced by Na^+ ions that are coordinated by either 3 or 4 framework oxygen atoms. A significant proportion of the Al^{3+} in tetrahedral coordination exist in sites of lower symmetry, where some of the charge balancing capacity is provided by extra-framework Al species which have not previously been observed in these materials. The mean Si^{IV}-O-Al^{IV} bond angles for each type of Al^{IV} environment are highly consistent, with compositional changes dictating the relative proportions of individual Al^{IV} species but not altering the local structure of each individual Al^{IV} site. This model provides a more advanced description of the chemistry and structure of alkali aluminosilicate gels and is crucial in understanding, and controlling, the molecular interactions governing gel formation, mechanical properties and durability.

1. Introduction

Alkali aluminosilicate gels can be formed in an organic-free synthesis by reaction of an alkaline or alkali-silicate solution with a solid aluminosilicate precursor, and are characterized by a three-dimensionally crosslinked, structurally disordered, alkali aluminosilicate network. These materials have received significant academic and commercial interest in recent years due to desirable technical and environmental characteristics. Alkali aluminosilicate gels have potential for use in zeolite synthesis, in sol-gel processing, as low-cost refractories, as construction materials, in radioactive waste treatment, and in biomaterial and fiber composite applications.[1-3]

The nanostructure of alkali aluminosilicate gels primarily consist of an alkali aluminosilicate hydrate gel framework (abbreviated N-A-S-H, as Na is the most common alkali used) with a highly crosslinked, long-range disordered (X-ray amorphous), pseudo-zeolitic structure[4]. Al and Si are both present in tetrahedral coordination, analogous to their roles in zeolitic aluminosilicate frameworks, with Si existing in $Q^4(m\text{Al})$ environments; where *m* is between 1 and 4 depending on the Al/Si ratio of the gel, and Al is predominantly in $q^4(4\text{Si})$ environments due to the energetic penalty associated with Al^{IV}-O-Al^{IV} bonding[5]. The negative charge associated with Al substitution for Si is balanced by the alkali cations. This nanostructure can be significantly affected by kinetic limitations on silica and alumina release from solid precursors used in gel synthesis[6-7], and consequently evolves over time as the alkali-activation reaction proceeds.

Physicochemical, ion exchange, and mass transport properties of alkali aluminosilicate gels are controlled by the gel chemical composition and nanostructure, and the underlying phenomena controlling these interactions have received significant scientific attention in recent years.[8-10]. The way in which water is bound within the gel is of particular importance, as this determines the resistance to thermal processes, as well as structural changes related to variation in environmental humidity (e.g. microcracking).

Currently, knowledge of the N-A-S-H gel structure is primarily limited to average cation coordination spheres and bulk gel composition. This has created significant limitations in understanding the phase evolution, nanostructural development, and the fundamental physicochemical interactions which dictate the mechanical properties and durability of these materials.

A particularly attractive route to the synthesis of alkali aluminosilicate gels for nanostructural analysis is the reaction of high-purity synthetic amorphous precursors, themselves synthesized via an organic steric entrapment solution polymerization route, with an alkaline solution.[11-14] Study of these chemically simplified, high-purity systems under controlled conditions has yielded significant advances

in the understanding of gel nanostructural development due to the ability to isolate and control key parameters dictating these interactions, enabling selective isotopic labelling and avoiding any interference from contaminants. Analytical techniques including X-ray powder diffraction, vibrational spectroscopy and pair distribution function analysis have been key to recent developments in understanding the nanostructure of alkali aluminosilicate gels. However, the complex nature of these disordered and dynamic systems means that detailed information regarding their atomic structure is still elusive.

Solid state magic angle spinning nuclear magnetic resonance spectroscopy (solid state MAS NMR) investigations of ^{27}Al, ^{29}Si and ^{23}Na nuclei in alkali aluminosilicates have yielded information about the coordination states of Al, the connectivity of Si, and the charge-balancing role of Na.[15-22] While many studies utilizing ^{17}O MAS NMR have yielded important structural information regarding zeolites and aluminosilicate glasses, very few have probed ^{17}O nuclei in alkali aluminosilicate gels. This is, at least in part, due to the very low natural abundance (0.037%) of the NMR-active ^{17}O nucleus, which necessitates isotopic enrichment of samples.[23-24] Due to the disordered structure of alkali aluminosilicate gel frameworks, significant line broadening occurs at practically achievable MAS rates and consequently spectroscopic data for all relevant nuclei are usually poorly resolved. This is exacerbated for quadrupolar nuclei (spin $I > 1/2$) such as ^{27}Al ($I = 5/2$), ^{17}O ($I = 5/2$) and ^{23}Na ($I = 3/2$) which experience second order quadrupolar broadening that is not fully averaged by MAS.

Multiple quantum magic angle spinning (MQMAS) spectroscopy,[25-26] probing half integer quadrupolar nuclei including ^{17}O, ^{23}Na, and ^{27}Al, has been used to obtained high resolution NMR spectra of alkali aluminosilicate gels[20, 23-24, 27-28] and related reaction products[28-29]. MQMAS achieves high resolution by partially averaging the fourth-order Legendre polynomial through conversion of a symmetric multiple quantum coherence (pQ, p = 3,5,7,… for $p \leq 2I$) to the single quantum ($1Q$) detectable central transition, and plotting pQ and $1Q$ correlations in two dimensions.[23] Thus, chemical species with similar local structures and coordination environments, which would otherwise give overlapping resonances in 1D MAS NMR spectra, may be resolved on the basis of their quadrupolar interactions.

Here we use ^{27}Al, ^{23}Na and ^{17}O MAS and 3QMAS NMR spectroscopy to examine nanostructural development in a novel class of stoichiometrically controlled phase pure N-A-S-H gel frameworks synthesized previously[11, 13]. A range of shearing schemes are used in processing the 3QMAS spectroscopic data, to allow improved visualization of the isotropic chemical shift (δ_{iso}) from both the quadrupolar induced shift (δ_{QIS}) and the quadrupolar coupling constant (C_Q). The key structural motifs which assemble to form the N-A-S-H gel are identified and a new, self-consistent molecular model describing the structure of the N-A-S-H gel framework in alkali aluminosilicate gels is developed. Of

particular interest are the local coordination and nearest-neighbor environments of the key network-forming Si, Al and O atoms, network-modifying Na atoms, and associated H_2O molecules. This model establishes a new platform of knowledge which is crucial for developing further detailed understanding of the molecular interactions that govern the structure and properties of alkali aluminosilicate gels.

2. Experimental Procedures

2.1 Materials

The synthetic gels used in this study were produced by alkali-activation of high-purity synthetic aluminosilicate precursor powders previously synthesized using an organic steric entrapment solution-polymerization method (further details are provided in Appendix A Supporting Information).[11] Detailed analysis of phase evolution and microstructural development of these gels over 224 days has been previously published.[11] The gels to be examined using ^{17}O 3QMAS NMR spectroscopy were produced with an isotopically enriched activating solution prepared by dissolution of sodium metasilicate powder (Na_2SiO_3, Sigma Aldrich) in 41.1 wt. % $H_2{}^{17}O$ (Cortecnet). The stoichiometry was designed to obtain an activating solution modulus (molar ratio SiO_2/Na_2O) = 1, a total isotopic enrichment of 26 - 31 wt. %, and cation ratios as outlined in Table 1. The activating solution (pH> 13.5) was stored for 72 hours to allow equilibration and facilitate maximum oxygen isotopic exchange into the dissolved silicate species, then mixed with the precursor powder to form a homogeneous paste which was cast in sealed containers and cured at ambient temperature for 7 days. Before analysis by NMR, each gel was ground by hand using a mortar and pestle and immersed in acetone to remove loosely bound water and halt reaction. This method does not induce any significant changes in the alkali aluminosilicate gel structure[30].

Table 1: Molar compositions and water/solid (w/s) mass ratios of the precursor and gel reaction mix for each sample

Sample	Empirical formula	Si/Al	Na/Al	w/s
Precursor A	$2SiO_2{\cdot}Al_2O_3$	1.00	0.00	0.00
Precursor B	$4SiO_2{\cdot}Al_2O_3$	2.00	0.00	0.00
Gel A	$1.18Na_2O{\cdot}3SiO_2{\cdot}Al_2O_3$	1.50	1.18	0.75
Gel B	$1.18Na_2O{\cdot}5SiO_2{\cdot}Al_2O_3$	2.50	1.18	0.75

2.2 Solid state nuclear magnetic resonance spectroscopy

All MAS and 3QMAS data were obtained at 14.1 T using a Bruker Avance II+ spectrometer at a Larmor frequency of 156.2 MHz, 158.6 MHz and 81.26 MHz for ^{27}Al, ^{23}Na and ^{17}O, respectively, and a Bruker 3.2 mm double air-bearing probe calibrated to yield a MAS frequency of 20 kHz. ^{27}Al MAS spectra were acquired using a 1 µs selective (π/9) excitation pulse, a measured 1 s relaxation delay and a total of 4096 transients, while ^{27}Al 3QMAS experiments were acquired using a 4.5 µs non-selective triple quantum excitation pulse followed by a 1.5 µs non-selective conversion pulse and a selective 20 µs z-filter pulse. All ^{27}Al MAS and 3QMAS spectra are aligned with the secondary reference yttrium aluminum garnet ($\delta_{iso}(AlO_6)$ = 0.7 ppm with respect to 1.1 M $Al(NO_3)_{3\ (aq)}$ = 0 ppm). ^{23}Na MAS spectra were acquired using a 1 µs non-selective (π/4) excitation pulse, a measured 1 s relaxation delay and a total of 4096 transients, while ^{23}Na 3QMAS experiments were acquired using a 4.0 µs non-selective triple quantum excitation pulse followed by a 1.2 µs non-selective conversion pulse and a selective 20 µs z-filter pulse. All ^{23}Na MAS and 3QMAS spectra are aligned with the secondary reference sodium chloride ($\delta_{iso}(NaCl_{(s)})$ = 7.2 ppm with respect to 1 M $NaCl_{\ (aq)}$ = 0 ppm). ^{17}O MAS spectra were acquired using a 1.75 µs non-selective (π/2) excitation pulse, a measured 1 s relaxation delay and a total of 2048 transients, while ^{17}O 3QMAS experiments were acquired using a 7.0 µs non-selective triple quantum excitation pulse followed by a 2.0 µs non-selective conversion pulse and a selective 17.5 µs z-filter pulse. All ^{17}O MAS and 3QMAS spectra are referenced to $H_2{}^{17}O$ at 0 ppm.

All 3QMAS spectra were processed by performing 2D Fourier transformations and shearing in the (δ_{3Q}, δ_{1Q}) axes using four different shearing functions. Iso-sheared spectra were sheared by a factor of (-*k*, 0) to give 2D spectra with an isotropic component along the δ_{3Q} (F1) axis and an anisotropic component along the δ_{1Q} (F2) axis,[31] while Q-sheared spectra were sheared by a factor of (*p*, 0) to remove the isotropic chemical shift from the indirect dimension to give a pure quadrupolar component (which purely reflects the second-order quadrupolar broadening and δ_{QIS}) along the δ_{3Q} axis, with an anisotropic component along the δ_{1Q} axis.[32-33] Biaxial shearing of the spectra was also performed, using either a factor of (-*k*, 1/(*p*+*k*)) to completely remove the isotropic chemical shift from the direct dimension and align the isotropic chemical shift axis (CS) perpendicular to that of the second-order quadrupolar broadening (biaxial iso-shearing),[23] or a factor of (*p*, -1/(*p*+*λ*)) so that the δ_{1Q} axis purely reflects the isotropic chemical shift and the quadrupolar parameters are separated in the δ_{3Q} axis (biaxial Q-shearing).[23] In each case, for a 3QMAS experiment, *k* = -19/12 and *p* = 3 for spin *I* = 5/2, or *k* = 7/9 and *p* = -3 for spin *I* = 3/2, and *λ* can be determined from the Glebsch-Gordan-derived coefficients.[23, 34] Gradients for each NMR parameter were determined from first principles as described previously[23] and are detailed in Table 2.

Anisotropic slices of each iso-sheared 3QMAS spectra were taken at the center of gravity of each resonance, and simulated using DMFit[35-36] and the Czjzek Gaussian Isotropic Model[37] with the minimum number of peaks to obtain a reasonable fit to the data and determine δ_{iso} and C_Q. These parameters were then used as a starting point to simulate each 1D MAS spectrum and obtain δ_{iso} and C_Q for each resonance. The δ_{iso} is also determined from the observed chemical shifts in the indirect (δ_1) and direct (δ_2) dimensions using equation 1.[29]

$$\delta_{iso}=\frac{17\delta_1+10\delta_2}{27} \quad (1)$$

Table 2: The gradients of NMR parameter axes (isotropic chemical shift CS, isotropic quadrupolar shift Q_{IS}, and anisotropic orientation dependent frequencies A) after shearing in the δ_{3Q}, δ_{1Q} dimension by the factors listed below, for a reversed directly detected dimension. Slopes were determined from first principles as described previously[23].

		***-k*, 0**	***-k*, 1/(*p*+*k*)**	***p*, 0**	***p*, -1/(*p*+λ)**
Spin	**Parameter**	**19/12, 0**	**19/12, 12/17**	**3, 0**	**3, -4/9**
5/2	CS	17/12	1/0	0	0
	Q_{IS}	-5/6	-85/162	-9/4	1/0
	A	0	0	-17/12	-153/40
Spin	**Parameter**	**-7/9, 0**	**-7/9, 34/9**	**-3, 0**	**-3, -1/6**
3/2	CS	34/9	1/0	0	0
	Q_{IS}	-20/9	-340/243	-6	1/0
	A	0	0	-34/9	-51/5

3. Results and discussion

3.1 ^{27}Al MAS and 3QMAS NMR

The ^{27}Al MAS NMR spectra of the precursors and synthetic gels do not provide sufficient resolution to allow identification of individual environments, beyond general identification of Al coordination environments, and show no significant differences between samples. This is typical of disordered materials where the variable environments coupled with a variation in bond angles surrounding the nuclear site give a spread of the NMR parameters (δ_{iso}, C_Q and η_Q). A detailed discussion and interpretation of ^{27}Al MAS NMR spectra for these precursors and gels collected at a 10 kHz MAS rate has been previously published[11, 13], and the spectral distributions visible here are consistent with those identified in that study.

Iso-sheared ^{27}Al 3QMAS NMR spectra for the aluminosilicate precursors and gels, along with projections along the δ_{1Q} and δ_{3Q} axes, are presented in Figure 1. A broad distribution of resonances

in each of the Al^{IV}, Al^{V} and Al^{VI} regions of the spectra (centered, δ_{cg}, at approximately (74 ppm, 67 ppm), (43 ppm, 37 ppm) and (12 ppm, 7 ppm) in the ($\delta_{3Q,\,cg}$, $\delta_{1Q,\,cg}$) axes, respectively) is observed for both precursors. Broadening of the Al^{IV} resonances occurs primarily along the CS axis, suggesting that a distribution of isotropic chemical shifts is the main factor causing broadening of Al^{IV} resonances in these precursors. However, there is also significant broadening of the Al^{IV} resonance in the spectra of precursor A along the Q_{IS} axis, which indicates that a distribution of quadrupolar parameters contributes to signal broadening here. This is also indicated by the absence of any resolved second-order quadrupolar pattern.

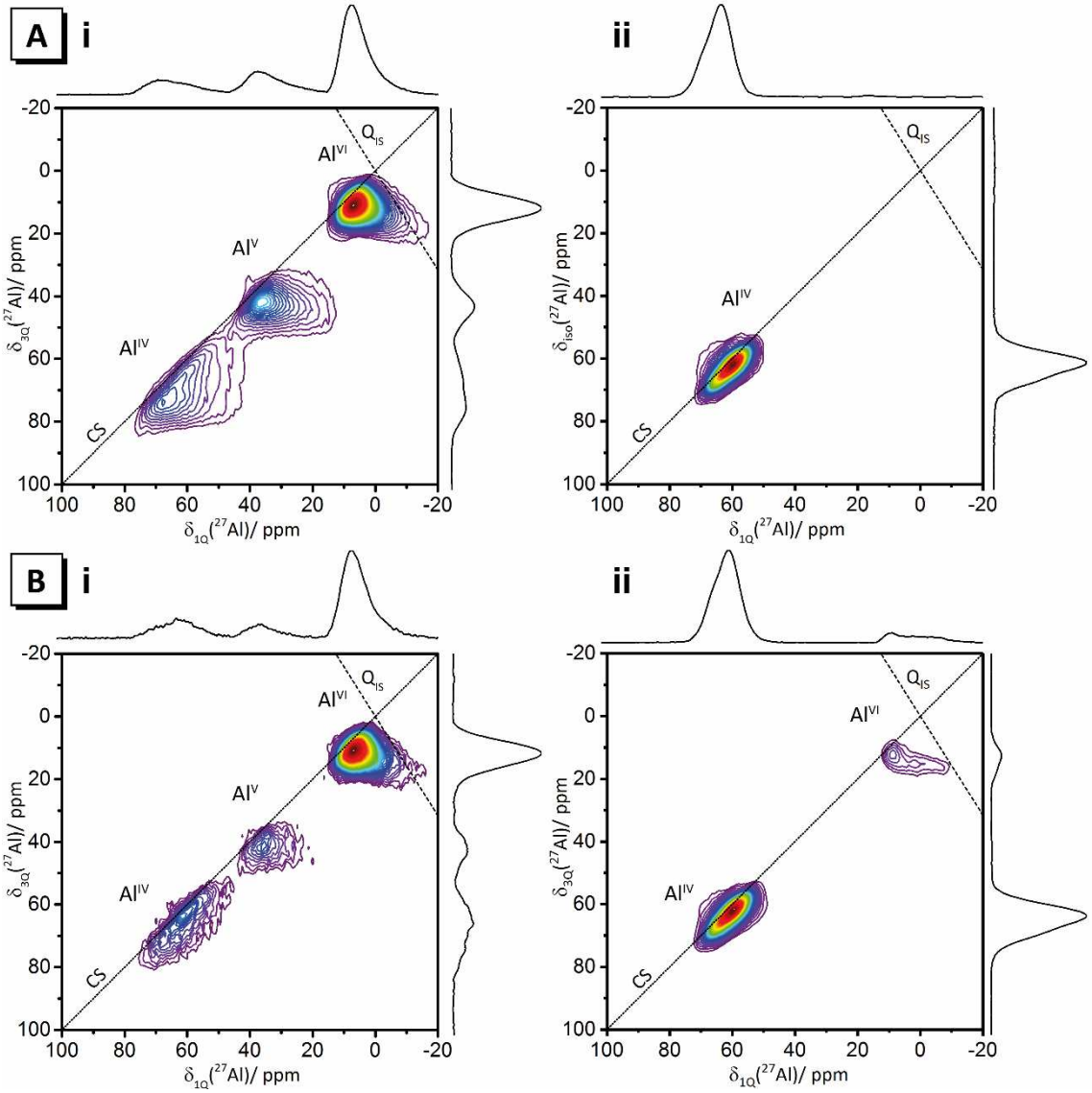

Figure 1: ^{27}Al 3QMAS NMR spectra of i) precursor and ii) alkali aluminosilicate gel, for samples A and B as marked. The spectra are sheared using conventional single axial iso-shearing in the δ_{3Q}, δ_{1Q} axes by a factor of 19/12, 0, respectively, to give an isotropic component in the δ_{3Q} (F1) dimension and the MAS 1D spectrum in the δ_{1Q} (F2) dimension. The chemical shift (CS) and quadrupolar induced shift (Q_{IS}) axes are indicated by dotted and dashed lines, respectively.

The observation of two local maxima in the Al^{IV} region of the projection onto the isotropic (δ_{3Q}) dimension (Figure 1 a i) suggests that there may be two overlapping distributions of Al chemical shifts (and hence two average Al^{IV} environments) within the precursor A, however this cannot be determined unambiguously from the single axial iso-sheared spectrum (Figure 1). The distribution of chemical shifts suggests a highly disordered Al^{IV} environment with a significant distribution of Si^{IV}-O^{-}-Al^{IV} valence angles and significant variation in the size and charge of the associated charge balancing cations (so as to induce a distribution of quadrupolar parameters). Quadrupolar broadening of the Al^{IV} resonance toward higher frequencies, approximately 80 ppm, may result from charge-balancing by cationic aluminum species (tentatively identified as Al^{V} or Al^{VI} species[11]) which significantly distort the electric field surrounding the Al nucleus.[38] A single resonance is observed in each of the Al^{V} and Al^{VI} regions of the iso-sheared spectra for the precursor A, exhibiting both chemical shift and quadrupolar broadening, and again suggesting the presence of disordered environments with significant variation of Al nuclear electrical field symmetry.

The Al^{IV} and Al^{V} regions of the spectrum of precursor B are primarily broadened along the CS axis and display minimal broadening along the Q_{IS} axis, suggesting that the species responsible for quadrupolar broadening in precursor A (tentatively identified above Al^{V} or Al^{VI} species in mullite-like environments) are not present, or minimal, in precursor B. This is consistent with the chemistry of the precursors (Si/Al = 1 and 2 for A and B, respectively); the reduced Al content of precursor B results in a decrease in the degree of charge balancing by any Al^{V} or Al^{VI} species. The Al^{VI} resonance in the spectra of the precursor B exhibits significant quadrupolar broadening toward higher frequencies.

The iso-sheared ^{27}Al 3QMAS spectrum for gel A (Figure 1 a ii) displays a single resonance in the Al^{IV} region which is primarily broadened along the CS axis but also displays slight quadrupolar broadening along the Q_{IS} axis. An almost identical resonance is found in the corresponding spectrum for gel B (Figure 1 b ii). Both resonances are attributed to a single tetrahedral Al^{IV} site linked to tetrahedral Si via oxygen bridges (i.e. Si^{IV}-O^{-}-Al^{IV}). The characteristics of this resonance are similar to those attributed to Si^{IV}-O^{-}-Al^{IV} charge-balanced by Na^{+} in alkali aluminosilicate gels formed by the reaction of metakaolin with sodium metasilicate.[27]

Orthogonal separation of chemical shielding and quadrupolar broadening mechanisms can be visualized by processing the ^{27}Al 3QMAS spectra using biaxial Q-shearing[23] (Figure 2), where the horizontal projection is broadened by variations in chemical shift and the vertical projection is broadened by quadrupolar interactions. The ^{27}Al isotropic slices taken through the center of gravity of each resonance and extracted from the biaxial-Q sheared ^{27}Al 3QMAS spectra are shown in Figure 3.

The ^{27}Al isotropic slices for gels A and B (Figure 2 and Figure 3) show an asymmetric distribution of chemical shifts.

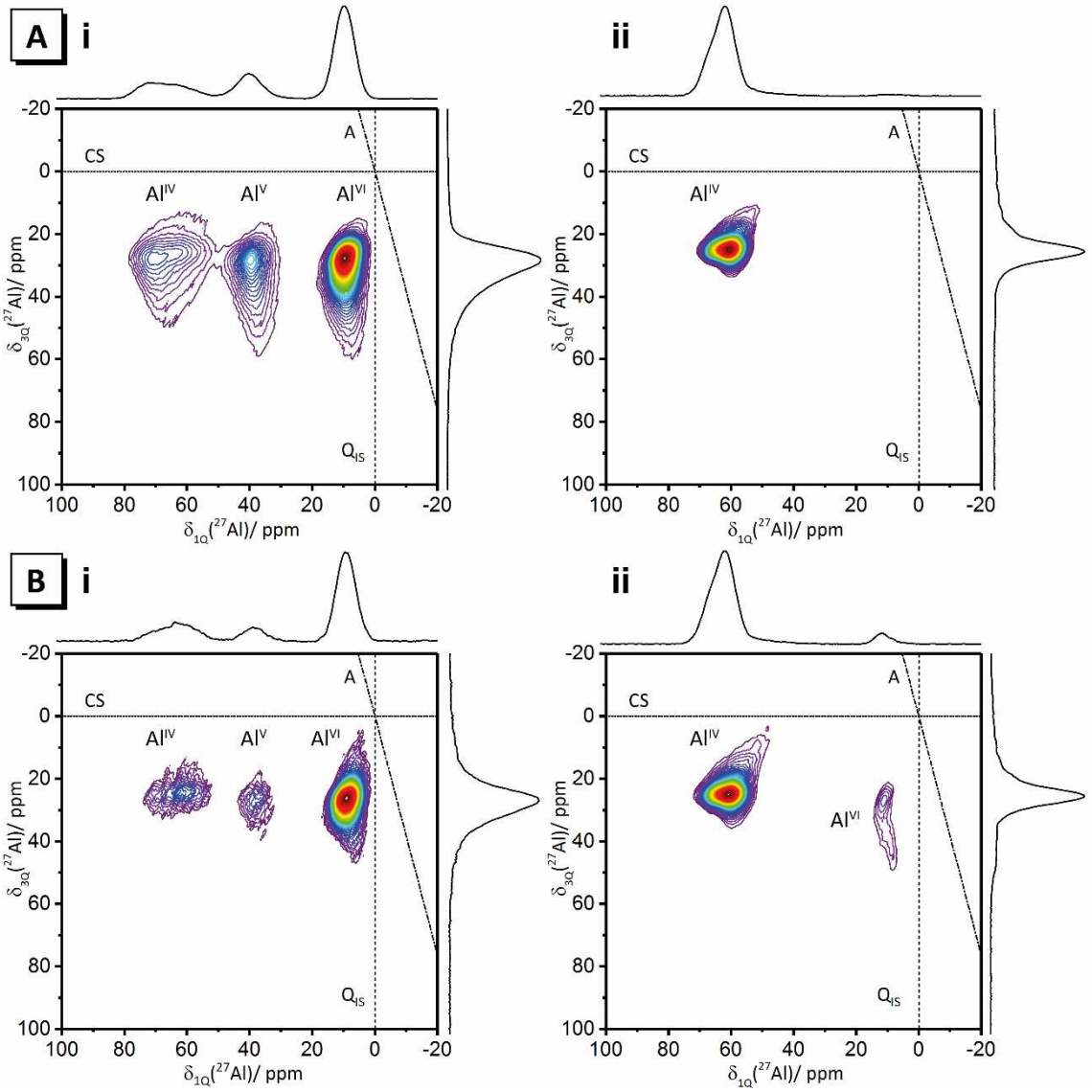

Figure 2: ^{27}Al 3QMAS NMR spectra of the i) precursor and ii) alkali aluminosilicate gel for samples A and B as marked. The spectra are sheared using biaxial Q-shearing in the δ_{3Q}, δ_{1Q} axes by a factor of 3, -4/9, respectively, so that the δ_{1Q} (F2) axis visualizes the isotropic chemical shift and the quadrupolar parameters are highlighted in the δ_{3Q} (F1) axis. The chemical shift (CS), quadrupolar induced shift (Q_{IS}) and anisotropic (A) axes are indicated by dotted, dashed and combined dotted/dashed lines, respectively.

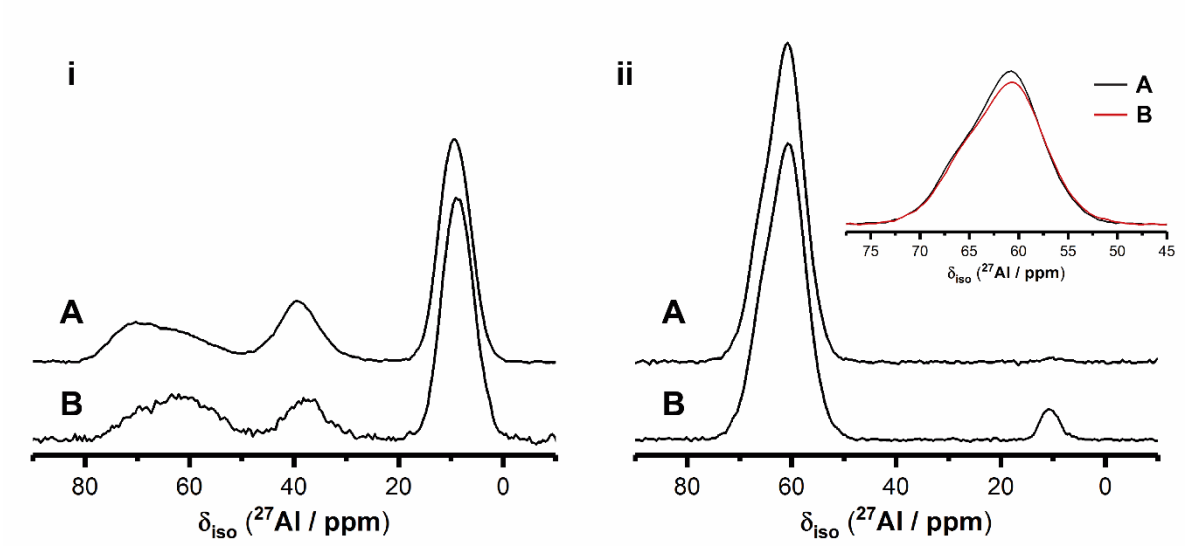

Figure 3: ^{27}Al isotropic slices, taken through the center of gravity of each resonance, extracted from the biaxial Q-sheared ^{27}Al 3QMAS NMR spectra of the i) precursor and ii) alkali aluminosilicate gel, for samples A and B as marked. The inset of ii) shows a rescaled plot of the Al^{IV} region of gel A (black) and B (red).

Two resonances are also observed within the Al^{VI} region of the biaxially Q-sheared ^{27}Al 3QMAS spectra for gel B (Figure 2 b i), both of which display smaller broadening along the CS axis, suggesting greater structural order and a narrower distribution of bond angles than precursor Al^{VI} sites. The shift of the lower intensity Al^{VI} resonance (Figure 2 b i) along the Q_{IS} axis toward higher frequencies suggests that it is associated with ionic species which induce large perturbations in the electric field gradient (EFG) surrounding the Al nucleus. These resonances differ primarily by quadrupolar broadening (i.e. perturbation of the EFG). Both resonances are assigned to newly formed octahedrally coordinated Al environments in paragonite, the formation of which has been observed in these gels previously by XRD[13].

Simulations of the ^{27}Al MAS spectra, with associated deconvolutions, are presented in Figure 4. The relative intensity, δ_{iso} and C_Q for each identified Al environment within the precursor and gel for samples A and B, as well as the mean Al-O$^-$-Si bond angle (α) for each Al^{IV} environment (calculated from the mean δ_{iso} using equation 2 [39]), are given in Table 3. Simulations of anisotropic slices for each resonance identified in the ^{27}Al 3QMAS spectra were used to obtain the δ_{iso} and C_Q of each resonance. These parameters were then used to guide simulation of the ^{27}Al MAS spectra, with the δ_{iso} and C_Q of each resonance being adjusted as necessary (to account for spectral differences which arise due to differences in phasing one dimensional and two dimensional spectra) to fit the data. Simulations of anisotropic slices are provided in Appendix B, Supporting Information. As both the precursors and gels

exhibit extensive disorder, the δ_{iso} and C_Q values provided in Table 3 indicate the average of a distribution of these parameters for each site.

$$\alpha = \frac{137 - \delta_{iso}}{0.532} \quad (2)$$

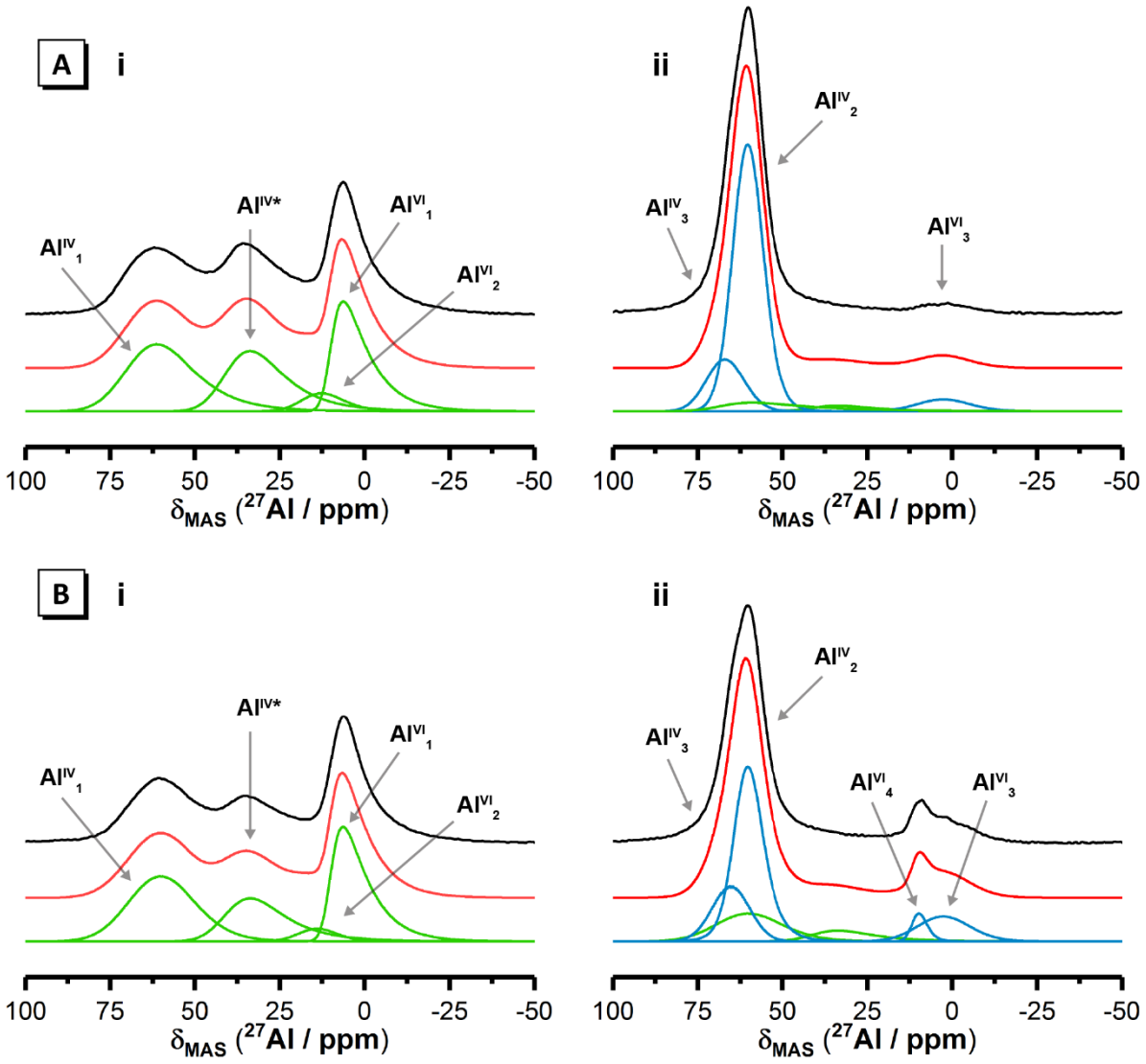

Figure 4: Deconvoluted ^{27}Al MAS NMR spectra of i) precursor and ii) alkali aluminosilicate gel for samples A and B as marked. Deconvoluted resonances (bottom curve) attributed to sites within the precursor are marked in green, deconvoluted resonances attributed to newly formed sites in the reaction product are marked in blue, the simulated spectrum is marked in red (middle curve) and the ^{27}Al MAS NMR spectrum is marked in black (top curve). The precursor simulations are utilized as a background for the simulations of the newly formed sites (ii).

Table 3: The NMR parameters extracted from the ^{27}Al 3QMAS spectra of the precursor and alkali aluminosilicate gel for each sample as marked. Here, $\delta_{1,cg}$ and $\delta_{2,cg}$ are the centers of gravity of the resonance in the isotropic (δ_{3Q}) and anisotropic (δ_{1Q}) dimensions, respectively; δ_{iso} is the isotropic chemical shift (Equation 1); and $\delta_{iso\ fit}$ and C_Q are the isotropic chemical shift and

quadrupolar coupling constant, respectively, obtained by simulating ^{27}Al MAS spectra with the asymmetry parameter (η) are fixed to zero. FWHM is full width at half maximum.

Sample	Site	Relative integral area (%)†	$\delta_{1,cg}$ (ppm)	$\delta_{2,cg}$ (ppm)	δ_{iso} (ppm)	$\delta_{iso,fit}$ (ppm)	FWHM (ppm)	C_Q (MHz)	Assignment	Si^{IV}-O-Al^{IV} bond angle‡
Precursor A_r	Al^{IV}_1	36	74.7	67.3	72.0	69.4	17.0	6.3	Al^{V} or Al^{VI} balanced Si^{IV}-O^--Al^{IV}	122.9
	Al^{IV}*	28	42.9	36.8	40.6	41.0	13.0	6.3	$AlO_4^-(T_3)$	-
	Al^{VI}_1	6	-	-	-	17.0	11.8	4.3	AlO_6	-
	Al^{VI}_2	30	11.7	7.1	10.0	10.5	5.0	5.5	AlO_6	-
Gel A	Al^{IV}_3	77	62.4	60.0	61.5	61.0	8.6	1.4	Na^+ balanced Si^{IV}-O^--Al^{IV}	143.4
	Al^{IV}_4	18	-	-	-	66.3	12.8	1.9	Na^+/Al_{EF} balanced Si^{IV}-O^--Al^{IV}	124.4
	Al^{VI}_3	6	15.7	-2.8	8.8	5.9	16.5	3.6	AlO_6	-
	Al^{VI}_4	-	-	-	-	-	-	-	AlO_6	-
Precursor B	Al^{IV}_1	37	73.2	68.5	71.5	66.0	20.0	4.9	Al^{V} or Al^{VI} balanced Si^{IV}-O^--Al^{IV}	122.2
	Al^{IV}*	23	42.7	35.9	40.2	41.0	13.0	6.3	$AlO_4^-(T_3)$	-
	Al^{VI}_1	4	-	-	-	17.0	11.8	3.5	AlO_6	-
	Al^{VI}_2	36	11.7	7.1	10.0	10.5	5.0	5.4	AlO_6	-
Gel B	Al^{IV}_3	59	62.8	60.0	61.7	61.0	8.6	1.4	Na^+ balanced Si^{IV}-O^--Al^{IV}	143.4
	Al^{IV}_4	22	-	-	-	66.3	12.8	1.9	Na^+/Al_{EF} balanced Si^{IV}-O^--Al^{IV}	124.4
	Al^{VI}_3	14	15.7	-2.8	8.9	5.9	16.5	3.6	AlO_6	-
	Al^{VI}_4	5	12.6	8.7	11.1	11.2	4.2	2.6	AlO_6	-

† The relative integrated intensity for each resonance for the gels is normalized to the sum of the sites within the reaction product. Residual precursor component contributions were observed in all gel spectra and are shown in Figure 4**,** but are excluded from the quantification of gel constituents.

‡ Equation 2 is only valid for tetrahedrally coordinated Al[39]

A single Al^{IV} environment exhibiting a broad distribution of chemical shifts is observed in the simulation and deconvolution of the ^{27}Al MAS spectra for the aluminosilicate precursors at δ_{iso} = 69.4 ppm (Al^{IV}_1). The C_Q value for this environment (6.3 MHz) indicates extensive perturbation of the electric field around the Al nuclei. Another environment at δ_{iso} = 41.0 ppm, also experiencing significant electric field perturbation (C_Q = 6.3 MHz) is observed in both precursors and assigned to distorted AlO_4^- sites in tricluster tetrahedra sharing a common oxygen atom (T_3, AlO_4^-), which have previously been observed in this region in ^{27}Al MAS NMR spectra of 3:2 mullite[38] and are likely to be present within mullite-like environments identified within the precursor aluminosilicates[11]. Two distinct Al^{VI} environments are also observed in each aluminosilicate precursor, at 17.0 and 10.5 ppm (Al^{VI}_1 and Al^{VI}_2, respectively) and are assigned to Al within mullite-like sites[38].

Deconvolution of the ^{27}Al MAS spectra for each gel required simulation of each MAS spectrum with two mean Al^{IV} resonances at $\delta_{iso} \approx 61.0$ (Al^{IV}_3) and 66.3 ppm (Al^{IV}_4) respectively. To confirm the presence of these two resonances, ^{27}Al isotropic slices were extracted from the biaxial Q-sheared ^{27}Al 3QMAS spectra, taken through the center of gravity of the Al^{IV} resonance (Figure 3). Two Gaussian distributions were required to satisfactorily fit the Al^{IV} resonance in the ^{27}Al isotropic slice for each gel, suggesting two overlapping distributions of chemical shielding.

The C_Q value of 1.4 MHz for the Al^{IV}_3 resonance in the ^{27}Al 3QMAS spectra shows a small electric field perturbation, indicating close association with low charge ionic species. This is consistent with the known environments of Al tetrahedra within Si^{IV}-O^--Al^{IV} linkages charge-balanced by Na^+ ions in these gels previously,[13] and in synthetic amorphous aluminosilicates[27] and zeolites.[40] The C_Q values for the Al^{IV}_4 resonance are larger (1.9 MHz) and this resonance exhibits a broader distribution of chemical shifts. The Al^{IV}_4 resonance may be due to lower symmetry Si^{IV}-O^--Al^{IV} linkages charge-balanced by Na^+ or extra-framework Al^{IV} species (Al_{EF}, e.g. $Al(OH)_2^+$ or $Al(OH)^{2+}$) which have been identified previously in zeolites[41-44]. Multiple overlapping ^{27}Al MAS and 3QMAS resonances due to two distributions of framework Al in zeolites has been previously observed.[45]

The mean Si-O-Al bond angles for the Na^+ balanced Si^{IV}-O^--Al^{IV} sites (143.4º) and the Na^+/Al_{EF} balanced Si^{IV}-O^--Al^{IV} sites (124.4º) and are identical across both alkali aluminosilicate gels, and are within the range observed for these sites within alkali-activated metakaolin[27]. The consistency of these bond angles suggests strong structural similarity between gel A and B, despite the differing initial Si/Ai molar ratios of the precursors.

3.2 ^{23}Na MAS and 3QMAS NMR

^{23}Na MAS NMR spectra for each gel each exhibit a broad resonance centered at approximately −3 ppm, attributed to sodium associated with aluminum tetrahedra in a charge balancing capacity within the N-A-S-H gel[13, 18, 21]. Due to the presence of multiple Si^{IV}-O^{-}-Al^{IV} sites identified by ^{27}Al 3QMAS above, it is possible that this broad resonance contains contributions from multiple Na sites with differing coordination spheres or proximities to each identified Si^{IV}-O^{-}-Al^{IV} site. Consequently, ^{23}Na 3QMAS spectra were obtained to further investigate these environments.

The iso-sheared ^{23}Na 3QMAS spectra for each gel (Appendix C, Supporting Information) each exhibit a moderately broad resonance centered at approximately (2.4 ppm, −3.0 ppm) in the ($\delta_{3Q,\,cg}$, $\delta_{1Q,\,cg}$) axes. The distributions of this resonance occurs to similar extents along the CS and Q_{IS} axes, which is typical for an electrostatic Na cation. A high frequency shoulder on the projection along the horizontal axis of the biaxial Q-sheared spectra (Figure 5) for both gels suggests that two distinct sites contribute to this resonance, and these are denoted Na^{+}_{1} and Na^{+}_{2}. A symmetrical distribution of quadrupolar parameters is observed for both gels.

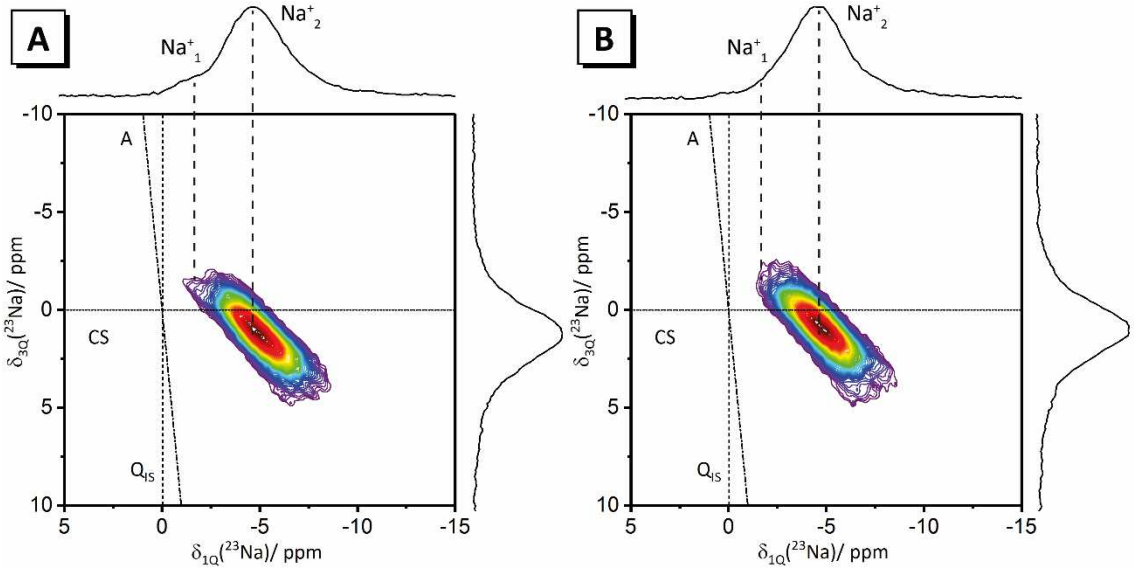

Figure 5: ^{23}Na 3QMAS NMR spectra of alkali aluminosilicate gels A and B as marked. The spectra are sheared using biaxial Q-shearing in the δ_{3Q}, δ_{1Q} axes by factors of (-3, -1/6), respectively, so that the δ_{1Q} (F2) axis purely reflects the isotropic chemical shift and the quadrupolar parameters are separated in the δ_{3Q} (F1) axis. The chemical shift (CS), quadrupolar induced shift (Q_{IS}) and anisotropic (A) axes are indicated by dotted, dashed and combined dotted/dashed lines, respectively.

The relative intensity, δ_{iso} and C_Q, for each identified Na environment within gel A and B (obtained by simulation of the ^{23}Na MAS spectra), as well as the average Na-O interatomic distance ($d_{\text{Na-O}}$, Å) for each sodium environment (calculated from δ_{iso} using Equation 3 [39]), are given in Table 4.

Deconvolutions of the ^{23}Na MAS spectra are provided in Figure 6, while simulations of anisotropic slices for each resonance identified in the ^{23}Na 3QMAS spectra were used to guide the simulation of the ^{23}Na MAS spectra are provided in Appendix C, Supporting Information. Again, it should be noted that as these gels exhibit extensive disorder, the δ_{iso} and C_Q values provided in Table 4 indicate the average distribution of these parameters for each site.

$$d_{\mathrm{Na-O}} = \frac{\delta_{\mathrm{iso}} - 179}{67} \quad (3)$$

Deconvolution of the ^{23}Na MAS spectra gives resonances located at $\delta_{iso} \approx$ -1.3 ppm and -2.7 ppm (for Na^+_1 and Na^+_2, respectively). The δ_{iso}, C_Q and $d_{Na\text{-}O}$ values for Na^+_1 are consistent with Na^+ ions charge-balancing Si^{IV}-O^--Al^{IV} linkages and coordinated by at least 3 framework oxygen atoms (with any remaining coordination position occupied by a water molecule) within an N-A-S-H gel, and are similar to those observed for Na^+ ions within amorphous aluminosilicate zeolite precursors[40] and alkali-activated metakaolin[27]. The C_Q value for Na^+_1 within gel A (1.41 MHz) is marginally less than that of gel B (1.57 MHz), showing slightly more perturbation of the EFG around the Na nuclei in gel B. This is likely to be due to the increased Si content of gel B causing an increased proportion of Si atoms surrounding the Na^+ cations. The δ_{iso} and C_Q values for Na^+_2 are consistent with those of hydrated Na^+ ions within relatively large aluminosilicate cages.[27]

From a geometric perspective, it is highly unlikely that the Na^+ ions within the disordered N-A-S-H gel will be coordinated entirely by framework oxygen atoms (in bridging positions in Si-O^--Al^{IV} linkages), meaning that Na^+ ions are also likely to be coordinated to water molecules[21, 27, 40]. In the gels analyzed here, the low isotropic chemical shift and large $d_{Na\text{-}O}$ value (2.67 Å) observed for the Na^+_1 site in both gels suggest that this Na^+ site is coordinated by at least 3 framework oxygen atoms, with any remaining coordination positions occupied by water molecules.[40] The Na^+_2 sites in these gels exhibit a lower isotropic chemical shift and a $d_{Na\text{-}O}$ distance 0.01 Å greater than that of the Na^+_1 site, suggesting that fewer H_2O molecules are present in the coordination sphere of Na atoms in this site,[40] signifying coordination to at least 4 framework oxygen atoms. This will result in less perturbation of the EFG surrounding the Na nuclei, consistent with the much lower C_Q values (0.70 MHz) observed for the Na^+_2 site.

Table 4: The ^{23}Na parameters extracted from the 3QMAS spectra alkali aluminosilicate gel for each gel. Quantities are as defined in Table 3, and spectral simulations were conducted with the asymmetry parameter η assumed to be zero.

Sample	Site	Relative integrated area (%)	$\delta_{1,cg}$ (ppm)	$\delta_{2,cg}$ (ppm)	δ_{iso} (ppm)	$\delta_{iso\ fit}$ (ppm)	C_Q (MHz)	Assignment	d_{Na-O} (Å), Eq. 3
Gel A	Na^+_1	58	2.39	-2.92	0.42	-1.26	1.41	Na^+ balancing Si^{IV}-O^--Al^{IV} coordinated by at least 3 bridging-O (balance H_2O)	2.67
	Na^+_2	42	0.37	-2.82	-0.81	-2.60	0.70	Na^+ balancing Si^{IV}-O^--Al^{IV} coordinated by 4 bridging-O (balance H_2O)	2.68
Gel B	Na^+_1	63	2.42	-3.15	0.36	-1.42	1.57	Na^+ balancing Si^{IV}-O^--Al^{IV} coordinated by at least 3 bridging-O (balance H_2O)	2.67
	Na^+_2	37	-0.03	-2.10	-0.80	-2.83	0.70	Na^+ balancing Si^{IV}-O^--Al^{IV} coordinated by 4 bridging-O (balance H_2O)	2.68

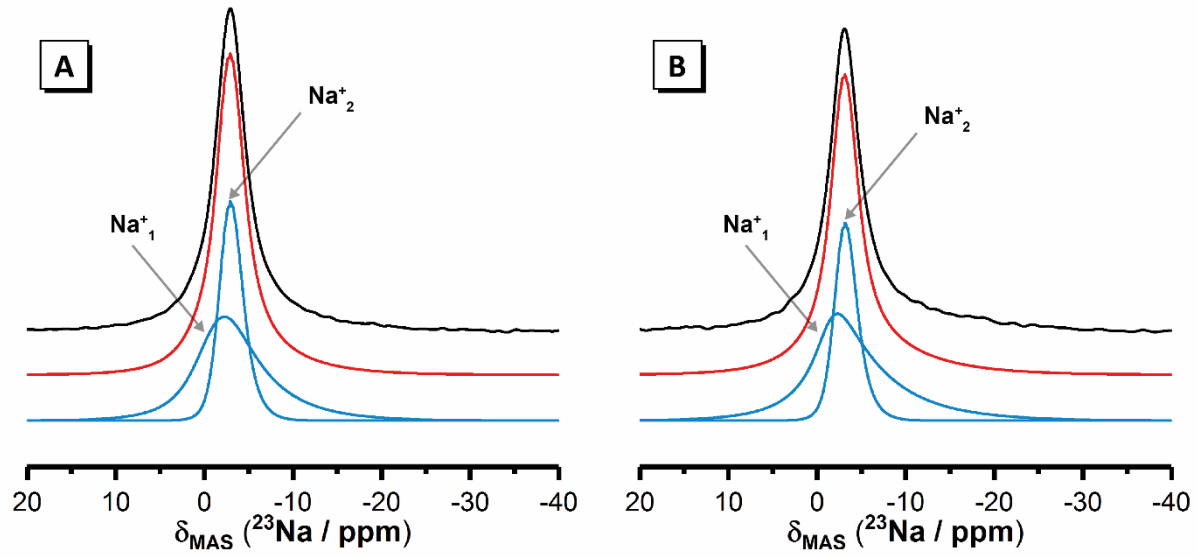

Figure 6: Deconvoluted ^{23}Na MAS NMR spectra for the alkali aluminosilicate gels A and B, as marked. Deconvoluted resonances are marked in blue (bottom curve), the simulated spectrum is marked in red (middle curve) and the ^{23}Na MAS NMR spectrum is marked in black (top curve).

3.3 ^{17}O MAS and 3QMAS NMR

The ^{17}O MAS NMR spectra for each gel (Figure 7) gives a broad large intensity resonance centered at approximately (δ_{cg}) 34 ppm which is attributed to bridging oxygen within the aluminosilicate gel

framework.[46-47] Due to extensive line broadening this resonance extends across a region in which Si^{IV}-O^{-}-Si^{IV}, Si^{IV}-O-Al^{IV} and Al^{IV}-O-Al^{IV} linkages have been observed.[48-49] A secondary lower intensity resonance is also observed, centered at approximately -10 ppm and -4 ppm in gels A and B, respectively, which is attributed to non-bridging oxygen atoms in Si-OH and Al-OH sites, as well as H_2O molecules tightly bound within the N-A-S-H gel.[46, 50]

The ^{17}O 3QMAS spectrum of each gel (Figure 8) exhibits a single resonance at approximately (35.0 ppm, 48.3 ppm) and (28.7 ppm, 47.8 ppm) in the ($\delta_{1Q,\,cg}$, $\delta_{3Q,\,cg}$) axes for each gel. This resonance is broadened primarily along the CS axis and tails off along the QIS axis suggesting the possibly of two distributions spanning the bridging region. An asymmetric distribution of isotropic chemical shifts is observed for this resonance in the ^{17}O isotropic slices extracted from the biaxial Q-sheared ^{17}O 3QMAS spectra (provided in Appendix D, Supporting Information). These resonances are consistent with those observed for Si^{IV}-O^{-}-Si^{IV} and Si^{IV}-O^{-}-Al^{IV} linkages in natural and synthetic zeolites[45-47, 51], and are attributed to bridging oxygen within these environments in a highly polymerized N-A-S-H gel. The resonances overlap, and show significant broadening along the CS axis, indicating a significant variation in Si^{IV}-O^{-}-Si^{IV} and Si^{IV}-O-Al^{IV} bond angles, consistent with the disordered nature of both N-A-S-H gels A and B. Moderate broadening occurs parallel to the Q_{IS} axis, indicating a distribution of quadrupolar parameters and variation in the symmetry of the EFG surrounding each oxygen atom.

If present, Al^{IV}-O-Al^{IV} linkages would exhibit a resonance at approximately 17 ppm in the direct dimension, and 25 ppm in the indirect dimension, of the iso-sheared spectra[47, 52-53]. Resonances in this region are not observed in the spectra for either gel, indicating that they follow Loewenstein's principle of Al-O-Al avoidance[54]. This is consistent with the chemistry of each gel (Al/Si < 1), whereas Al^{IV}-O-Al^{IV} bonds have been observed via ^{17}O 3QMAS NMR in synthetic N-A-S-H gels at Al/Si = 1.00 [24].

Deconvoluted ^{17}O MAS spectra (Figure 7) for each gel exhibit three distinct resonances (Table 5). The C_Q values for the resonance at $\delta_{iso} \approx 30.0$ ppm is small (C_Q = 1.00 MHz) indicating little electric field perturbation and close association with low charge ionic species. C_Q values for the resonances at $\delta_{iso} \approx 38.0$ ppm are notably larger (1.26 MHz) and indicate close association with species with greater charge. This agrees with the assignment of the resonance at $\delta_{iso} \approx 30.0$ ppm to Si^{IV}-O-Al^{IV} linkages and that at 38.0 ppm to Si^{IV}-O^{-}-Si^{IV} linkages, as connection to Si will induce greater disturbance of the EFG around the O nucleus than connection to Al^{3+} [55-56]. It is likely that the resonance at $\delta_{iso} \approx 30.0$ ppm contains contributions from oxygen within both the Na^{+} balanced Si^{IV}-O-Al^{IV} linkages and the lower symmetry Na^{+}/Al_{EF} balanced Si^{IV}-O-Al^{IV} linkages (identified by ^{27}Al 3QMAS NMR). The resonance at $\delta_{iso} \approx -10.0$ ppm is assigned to non-bridging oxygen present within Si-OH and Al-OH sites as well as tightly bound H_2O molecules within the aluminosilicate gel.[46, 50]

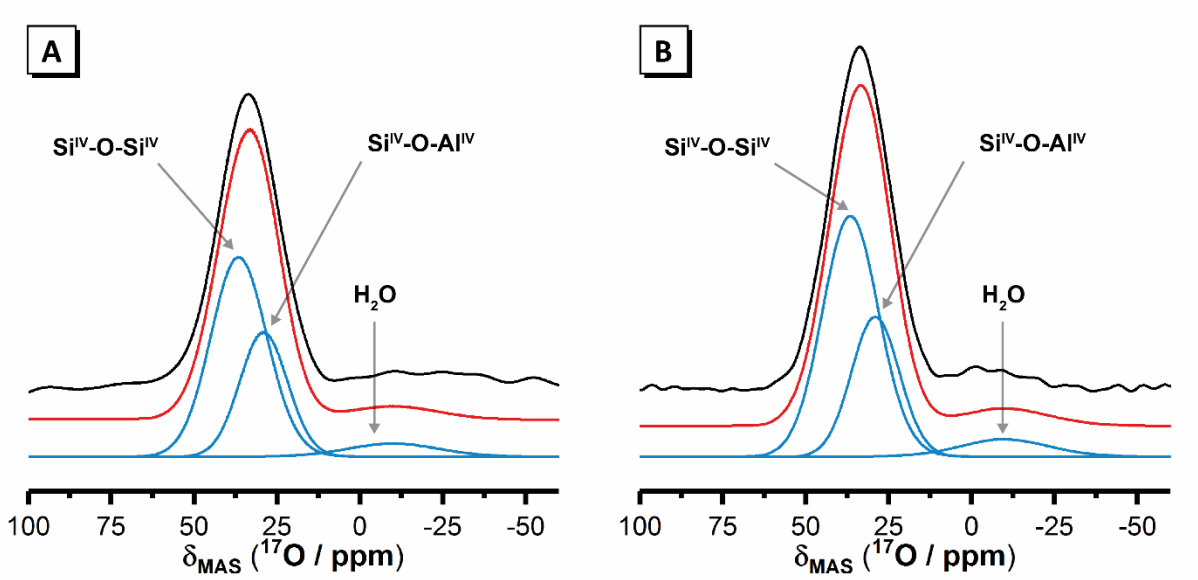

Figure 7: Deconvoluted ^{17}O MAS NMR spectra of the alkali aluminosilicate gels A and B, as marked. Deconvoluted resonances are marked in blue (bottom curve), the simulated spectrum is marked in red (middle curve) and the ^{17}O MAS NMR spectrum is marked in black (top curve). The spectral simulations show the expected positions of the BO and NBO environments as given in the 3QMAS data.

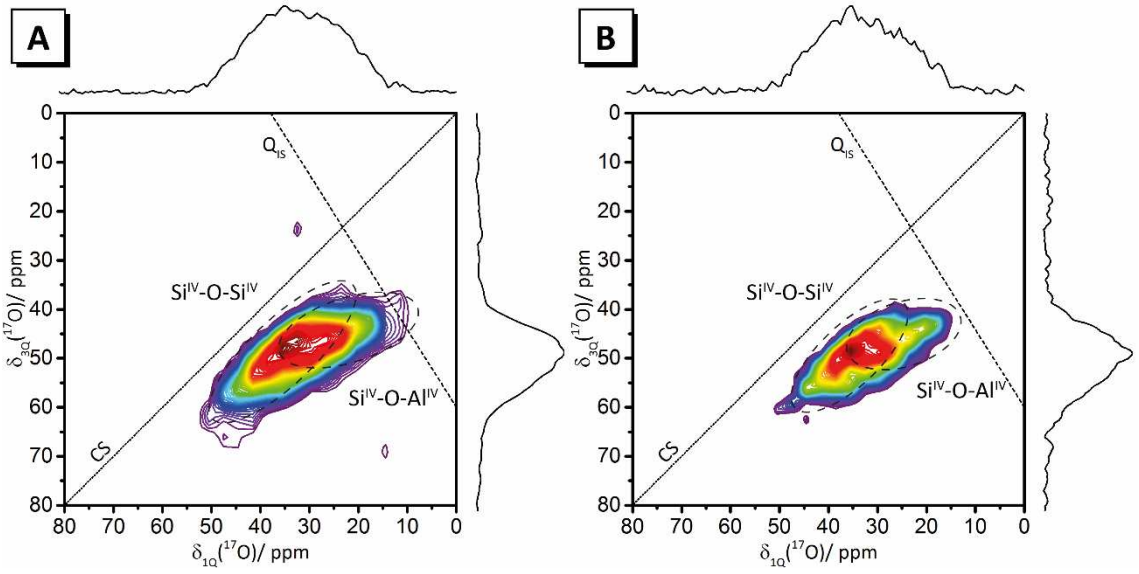

Figure 8: ^{17}O 3QMAS NMR spectra of alkali aluminosilicate gels A and B, as marked. Spectra are sheared using conventional single axial iso-shearing in the δ_{3Q}, δ_{1Q} axes by a factor of 19/12, 0, respectively, to give an isotropic component in the δ_{3Q} (F1) dimension and an anisotropic component in the δ_{1Q} (F2) dimension. The chemical shift (CS) and quadrupolar induced shift (Q_{IS}) axes are indicated by dotted and dashed lines, respectively. The assignments show the expected positions of the BO and NBO environments, the Si-O-Al BO typically are more Q_{IS} distributed and hence appear at a more horizontal position on the spectrum.

Table 5: ^{17}O parameters extracted from the 3QMAS spectra for each alkali aluminosilicate gel. Quantities are as defined in Table 3, and spectral simulations were conducted with the asymmetry parameter η assumed to be zero.

Sample	Site	Relative integral area (%)	$\delta_{1,cg}$ (ppm)	$\delta_{2,cg}$ (ppm)	δ_{iso} (ppm)	$\delta_{iso\ fit}$ (ppm)	C_Q (MHz)	Assignment
Gel A	1	61	48.3	35.0	43.4	39.0	1.26	Si-O^--Si
	2	32	-	-	-	33.0	1.00	Si-O^--Al^{IV}
	3	7	-	-	-	-9.8	0.55	H_2O
Gel B	1	62	48.6	34.3	43.7	39.0	1.26	Si-O^--Si
	2	31	-	-	-	33.0	1.00	Si-O^--Al^{IV}
	3	7	-	-	-	-9.8	0.55	H_2O

3.4 Structural model for the Na_2O-Al_2O_3-SiO_2-H_2O gel

Previous structural models have described the N-A-S-H gel formed by alkali-activation of aluminosilicate precursors as consisting of Al and Si tetrahedra randomly distributed in a polymerized network, with hydrated Na^+ ions associated with the AlO_4^- tetrahedra in a charge balancing capacity[20-21, 57]. Since these first broad descriptions, little further information has been obtained about individual chemical sites, or the distributions of bond angles or interatomic distances present within such gels.

Previous work involving ^{29}Si MAS NMR analysis of the gels studied here,[13] and of alkali-aluminosilicate gels produced from commercial precursors,[17, 58] has shown that Si within N-A-S-H gels exists exclusively in $Q^4(m\text{Al})$ environments where m is between 1 and 4 depending on the Al/Si ratio of the gel. In conjunction with this, the work presented here leads to the identification of six distinct recurring structural motifs which assemble to form the N-A-S-H gel (see Figure 9).

Three of these motifs are $Q^4(4\text{Al})$ Si units, in which the negative charge due to tetrahedrally coordinated Al is balanced by either:

- Na^+ ions coordinated by 3 framework (bridging) oxygen atoms and three H_2O molecules;
- Na^+ ions coordinated by 4 framework oxygen atoms and two H_2O molecules; or
- extra-framework Al atoms coordinated by 6 framework oxygen atoms.

The remaining motifs are $Q^4(m\text{Al})$ Si units, where m = 1, 2 or 3.

The relative integrated areas of each resonance within the deconvoluted ^{27}Al, ^{23}Na and ^{17}O MAS NMR spectra presented above, combined with previous ^{29}Si MAS NMR analysis of these gels (reproduced in Appendix E, Supporting Information), indicate that both N-A-S-H gels A and B are comprised of $Q^4(4Al)$, $Q^4(3Al)$, $Q^4(2Al)$ and $Q^4(1Al)$ Si units charge-balanced by Na^+ ions coordinated by either 3 or 4 framework oxygen atoms (with the balance H_2O molecules). A significant proportion (18 - 22%) of the Al^{3+} in tetrahedral coordination exist in a lower symmetry distribution where some of the charge balancing capacity is provided by extra-framework Al species. Increasing the Si/Al ratio (i.e. moving from the composition of gel A to gel B, Table 1) increases the number of Si^{IV}-O^--Si^{IV} linkages due to the presence of $Q^4(m\text{Al})$ Si units with $m < 4$.

The N-A-S-H gel contains a significant distribution of Si^{IV}-O^--Al^{IV} bond angles, with an average value of 143.4° and 124.4° in the Na^+ and Na^+/Al_{EF} balanced $Q^4(m\text{Al})$ Si units, respectively, as well as a significant distribution in chemical shifts and quadrupolar coupling parameters; Figure 9 shows these average values. This variability is also consistent with the absence of long range (crystalline) order. Due to these variations, bonds within the N-A-S-H gel may be significantly distorted, and consequently a structural model cannot extend for more than a few nearest neighbor species. A schematic and a three-dimensional representation of a section of the gel comprised for each of the main structural motifs, including details of average bond angles and interatomic distances where known, are shown in Figure 9.

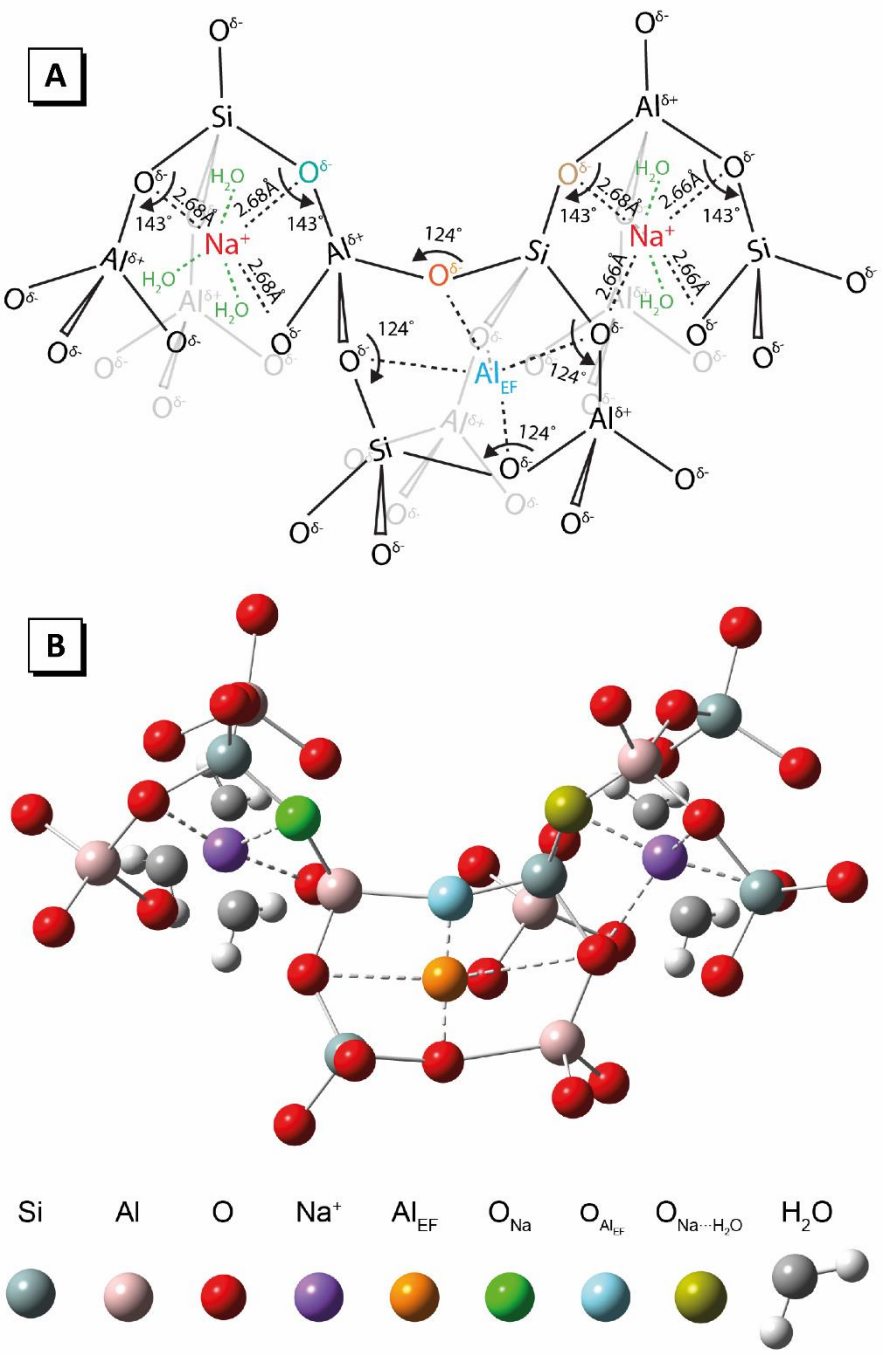

Figure 9: a) Schematic representation of a section of N-A-S-H gel showing charge balancing sodium, charge balancing Al_{EF}, bridging oxygen charge balanced by Na^+ and associated with three H_2O molecules, bridging oxygen charge balanced by Al_{EF} and bridging oxygen charge balanced by Na^+ and associated with three H_2O molecules; b) 3D representation of a polymerized section of the N-A-S-H gel showing each species as marked.

The findings presented in this study provide a new insight into complex, highly polymerized disordered N-A-S-H within alkali aluminosilicate gels. Changes in the Si/Al ratio of these gels dictate the proportion of each chemical species, and consequently the structure gel and physical properties of the binder.

With knowledge of nanostructural changes induced by manipulation of reaction mixture chemistry, as demonstrated in this study, it becomes possible to design tailor-made alkali aluminosilicate gels with specific physical properties and durability under a variety of applications and environments.

4. Conclusions

^{17}O enriched hydrous alkali aluminosilicate (N-A-S-H) gels have been produced via the reaction between a ^{17}O-enriched sodium silicate solution and high-purity synthetic aluminosilicate precursor powders. Application of ^{17}O, ^{23}Na and ^{27}Al 3QMAS NMR spectroscopy has enabled the identification of six key structural motifs present within N-A-S-H in alkali aluminosilicate gels of differing Si/Al ratios, which were combined to develop a new structural model of the N-A-S-H gel framework.

Three of these motifs are $Q^4(4Al)$ Si units, in which the negative charge due to tetrahedrally coordinated Al is balanced by either Na^+ ions coordinated by three framework oxygen atoms and three H_2O molecules; Na^+ ions coordinated by four framework oxygen atoms and two H_2O molecules; or by extra-framework Al atoms coordinated by six framework oxygen atoms. The remaining motifs are $Q^4(3Al)$, $Q^4(2Al)$ and $Q^4(1Al)$ Si units.

The N-A-S-H gel is comprised of $Q^4(4Al)$, $Q^4(3Al)$, $Q^4(2Al)$ and $Q^4(1Al)$ Si units charge-balanced by Na^+ ions coordinated by either three or four framework oxygen atoms. A significant proportion (18 - 22%) of the Al^{3+} in tetrahedral coordination exist in a lower symmetry distribution, where some of the charge balancing capacity is provided by extra-framework Al species. This has not been previously observed in alkali aluminosilicate gel systems.

The findings presented in this study, and the advanced structural description developed from these findings, establish a new platform of knowledge which is crucial for developing further detailed understanding of the molecular interactions governing phase evolution and nanostructural development of alkali aluminosilicate gels. This has significant implications regarding the durability of these materials, which will be useful for development of tailor-made alkali aluminosilicate gels with specific physical properties.

5. Supporting Information

Additional figures (S1-S13) as discussed in the main text.

6. Acknowledgements

This work has been funded in part by the Australian Research Council (ARC), including support through the Particulate Fluids Processing Centre, a Special Research Centre of the ARC. The University of Melbourne also provided support through an Overseas Research Experience Scholarship to support an extended visit by the first author to the University of Sheffield. B.W. wishes to thank and acknowledge Dr John Gehman, Gehman Lab Analytics Studio, for very helpful discussions regarding biaxial shearing of 3QMAS spectra. The participation of JLP has been supported by the Engineering and Physical Sciences Research Council (UK) through grant EP/M003272/1. The NMR Facility in Millburn House used in this research was funded by EPSRC, BBSRC, the University of Warwick and the Birmingham Science City Advanced Materials Projects 1 and 2, and supported by Advantage West Midlands and the European Regional Development Fund.

7. Conflicts of interest

There are no conflicts to declare

8. References

1. Provis, J. L.; Bernal, S. A., Geopolymers and Related Alkali-Activated Materials. *Annual Review of Materials Research* **2014**, *44*, 299-327.
2. Dent Glasser, L. S., Osmotic Pressure and the Swelling of Gels. *Cement and Concrete Research* **1979**, *9*, 515-517.
3. Dent Glasser, L. S.; Harvey, G., The Gelation Behaviour of Aluminosilicate Solutions Containing Na^+, K^+, Cs^+, and Me_4N^+. *Journal of the Chemical Society, Chemical Communications* **1984**, 1250-1252.
4. Provis, J. L.; Palomo, A.; Shi, C. J., Advances in Understanding Alkali-Activated Materials. *Cement and Concrete Research* **2015**, *78*, 110-125.
5. Provis, J. L.; Duxson, P.; Lukey, G. C.; van Deventer, J. S. J., Statistical Thermodynamic Model for Si/Al Ordering in Amorphous Aluminosilicates. *Chemistry of Materials* **2005**, *17*, 2976-2986.
6. Hajimohammadi, A.; Provis, J. L.; van Deventer, J. S. J., Effect of Alumina Release Rate on the Mechanism of Geopolymer Gel Formation. *Chemistry of Materials* **2010**, *22*, 5199-5208.
7. Hajimohammadi, A.; Provis, J. L.; van Deventer, J. S. J., The Effect of Silica Availability on the Mechanism of Geopolymerisation. *Cement and Concrete Research* **2011**, *41*, 210-216.
8. Zhang, Z.; Wang, H.; Provis, J. L.; Bullen, F.; Reid, A.; Zhu, Y., Quantitative Kinetic and Structural Analysis of Geopolymers. Part 1. The Activation of Metakaolin with Sodium Hydroxide. *Thermochimica Acta* **2012**, *539*, 23-33.
9. Bortnovsky, O.; Dědeček, J.; Tvarůžková, Z.; Sobalík, Z.; Šubrt, J., Metal Ions as Probes for Characterization of Geopolymer Materials. *Journal of the American Ceramic Society* **2008**, *91*, 3052-3057.
10. Fernández-Jiménez, A.; Monzó, M.; Vicent, M.; Barba, A.; Palomo, A., Alkaline Activation of Metakaolin–Fly Ash Mixtures: Obtain of Zeoceramics and Zeocements. *Microporous and Mesoporous Materials* **2008**, *108*, 41-49.
11. Walkley, B.; San Nicolas, R.; Sani, M. A.; Gehman, J. D.; van Deventer, J. S. J.; Provis, J. L., Synthesis of Stoichiometrically Controlled Reactive Aluminosilicate and Calcium-Aluminosilicate Powders. *Powder Technology* **2016**, *297*, 17-33.
12. Walkley, B.; Provis, J. L.; San Nicolas, R.; Sani, M. A.; van Deventer, J. S. J., Stoichiometrically Controlled C–(A)–S–H/N–A–S–H Gel Blends Via Alkali-Activation of Synthetic Precursors. *Advances in Applied Ceramics* **2015**, *114*, 372-377.
13. Walkley, B.; San Nicolas, R.; Sani, M. A.; Gehman, J. D.; van Deventer, J. S.; Provis, J. L., Phase Evolution of Na_2O-Al_2O_3-SiO_2-H_2O Gels in Synthetic Aluminosilicate Binders. *Dalton Transactions* **2016**, *45*, 5521-35.
14. Walkley, B.; San Nicolas, R.; Sani, M.-A.; Rees, G. J.; Hanna, J. V.; van Deventer, J. S. J.; Provis, J. L., Phase Evolution of C-(N)-A-S-H/N-A-S-H Gel Blends Investigated Via Alkali-Activation of Synthetic Calcium Aluminosilicate Precursors. *Cement and Concrete Research* **2016**, *89*, 120-135.
15. Brus, J.; Abbrent, S.; Kobera, L.; Urbanová, M.; Cuba, P., Advances in ^{27}Al MAS NMR Studies of Geopolymers. *Annual Reports on NMR Spectroscopy* **2016**, *88*, 79-147.
16. Bernal, S. A.; Provis, J. L.; Walkley, B.; San Nicolas, R.; Gehman, J. D.; Brice, D. G.; Kilcullen, A. R.; Duxson, P.; van Deventer, J. S. J., Gel Nanostructure in Alkali-Activated Binders Based on Slag and Fly Ash, and Effects of Accelerated Carbonation. *Cement and Concrete Research* **2013**, *53*, 127-144.
17. Duxson, P.; Provis, J. L.; Lukey, G. C.; Separovic, F.; van Deventer, J. S., ^{29}Si NMR Study of Structural Ordering in Aluminosilicate Geopolymer Gels. *Langmuir : the ACS journal of surfaces and colloids* **2005**, *21*, 3028-36.
18. Duxson, P.; Lukey, G. C.; Separovic, F.; van Deventer, J. S. J., Effect of Alkali Cations on Aluminum Incorporation in Geopolymeric Gels. *Ind Eng Chem Res* **2005**, *44*, 832-839.
19. Fernández-Jiménez, A.; Palomo, A.; Sobrados, I.; Sanz, J., The Role Played by the Reactive Alumina Content in the Alkaline Activation of Fly Ashes. *Microporous and Mesoporous Materials* **2006**, *91*, 111-119.

20. Rowles, M. R.; Hanna, J. V.; Pike, K. J.; Smith, M. E.; O'Connor, B. H., ^{29}Si, ^{27}Al, ^{1}H and ^{23}Na MAS NMR Study of the Bonding Character in Aluminosilicate Inorganic Polymers. *Applied Magnetic Resonance* **2007**, *32*, 663-689.
21. Barbosa, V. F. F.; MacKenzie, K. J. D.; Thaumaturgo, C., Synthesis and Characterisation of Materials Based on Inorganic Polymers of Alumina and Silica: Sodium Polysialate Polymers. *International Journal of Inorganic Materials* **2000**, *2*, 309-317.
22. Criado, M.; Fernández-Jiménez, A.; Palomo, A.; Sobrados, I.; Sanz, J., Effect of the SiO_2/Na_2O Ratio on the Alkali Activation of Fly Ash. Part II: ^{29}Si MAS-NMR Survey. *Microporous and Mesoporous Materials* **2008**, *109*, 525-534.
23. Gehman, J. D.; Provis, J. L., Generalized Biaxial Shearing of MQMA NMR Spectra. *Journal of Magnetic Resonance* **2009**, *200*, 167-172.
24. Duxson, P. The Structure and Thermal Evolution of Metakaolin Geopolymers. The University of Melbourne, 2006.
25. Frydman, L.; Harwood, J. S., Isotropic Spectra of Half-Integer Quadrupolar Spins from Bidimensional Magic-Angle-Spinning NMR. *Journal of the American Chemical Society* **1995**, *117*, 5367-5368.
26. Medek, A.; Harwood, J. S.; Frydman, L., Multiple-Quantum Magic-Angle Spinning NMR: A New Method for the Study of Quadrupolar Nuclei in Solids. *Journal of the American Chemical Society* **1995**, *117*, 12779-12787.
27. Brus, J.; Kobera, L.; Urbanová, M.; Koloušek, D.; Kotek, J., Insights into the Structural Transformations of Aluminosilicate Inorganic Polymers: A Comprehensive Solid-State NMR Study. *The Journal of Physical Chemistry C* **2012**, *116*, 14627-14637.
28. Faucon, P.; Charpentier, T.; Bertrandie, D.; Nonat, A.; Virlet, J.; Petit, J. C., Characterization of Calcium Aluminate Hydrates and Related Hydrates of Cement Pastes by ^{27}Al MQ-MAS NMR. *Inorganic chemistry* **1998**, *37*, 3726-3733.
29. Sideris, P. J.; Blanc, F.; Gan, Z.; Grey, C. P., Identification of Cation Clustering in Mg–Al Layered Double Hydroxides Using Multinuclear Solid State Nuclear Magnetic Resonance Spectroscopy. *Chemistry of Materials* **2012**, *24*, 2449-2461.
30. Ismail, I.; Bernal, S.; Provis, J.; Hamdan, S.; Deventer, J. J., Drying-Induced Changes in the Structure of Alkali-Activated Pastes. *Journal of Materials Science* **2013**, *48*, 3566-3577.
31. Massiot, D.; Touzo, B.; Trumeau, D.; Coutures, J. P.; Virlet, J.; Florian, P.; Grandinetti, P. J., Two-Dimensional Magic-Angle Spinning Isotropic Reconstruction Sequences for Quadrupolar Nuclei. *Solid state nuclear magnetic resonance* **1996**, *6*, 73-83.
32. Hung, I.; Trébosc, J.; Hoatson, G. L.; Vold, R. L.; Amoureux, J.-P.; Gan, Z., Q-Shear Transformation for MQMAS and STMAS NMR Spectra. *Journal of Magnetic Resonance* **2009**, *201*, 81-86.
33. Vold, R. L.; Hoatson, G. L.; Vijayakumar, M., Variable Temperature ^{93}Nb NMR Investigation of Local Structure and Polar Nanoclusters in Lead Magnesium Niobate/Lead Scandium Niobate Solid Solutions. *Physical Review B* **2007**, *75*, 134105.
34. Millot, Y.; Man, P. P., Procedures for Labeling the High-Resolution Axis of Two-Dimensional MQ-MAS NMR Spectra of Half-Integer Quadrupole Spins. *Solid state nuclear magnetic resonance* **2002**, *21*, 21-43.
35. Massiot, D.; Fayon, F.; Capron, M.; King, I.; Le Calvé, S.; Alonso, B.; Durand, J.-O.; Bujoli, B.; Gan, Z.; Hoatson, G., Modelling One- and Two-Dimensional Solid-State NMR Spectra. *Magnetic Resonance in Chemistry* **2002**, *40*, 70-76.
36. Neuville, D. R.; Cormier, L.; Massiot, D., Al Environment in Tectosilicate and Peraluminous Glasses: A ^{27}Al MQ-MAS NMR, Raman, and Xanes Investigation. *Geochimica et Cosmochimica Acta* **2004**, *68*, 5071-5079.
37. d'Espinose de Lacaillerie, J.-B.; Fretigny, C.; Massiot, D., MAS NMR Spectra of Quadrupolar Nuclei in Disordered Solids: The Czjzek Model. *Journal of Magnetic Resonance* **2008**, *192*, 244-251.

38. Rehak, P.; Kunath-Fandrei, G.; Losso, P.; Hildmann, B.; Schneider, H.; Jaeger, C., Study of the Al Coordination in Mullites with Varying Al:Si Ratio by ^{27}Al NMR Spectroscopy and X-Ray Diffraction. *American Mineralogist* **1998**, *83*, 1266-1276.
39. Mackenzie, K. J. D.; Smith, M. E., *Multinuclear Solid-State Nuclear Magnetic Resonance of Inorganic Materials*; Pergamon, Elsevier Science Ltd: Oxford, 2002.
40. Yang, H.; Walton, R. I.; Antonijevic, S.; Wimperis, S.; Hannon, A. C., Local Order of Amorphous Zeolite Precursors from ^{29}Si{^{1}H} CPMAS and ^{27}Al and ^{23}Na MQMAS NMR and Evidence for the Nature of Medium-Range Order from Neutron Diffraction. *The Journal of Physical Chemistry B* **2004**, *108*, 8208-8217.
41. Yu, Z.; Zheng, A.; Wang, Q.; Chen, L.; Xu, J.; Amoureux, J.-P.; Deng, F., Insights into the Dealumination of Zeolite HY Revealed by Sensitivity-Enhanced ^{27}Al DQ-MAS NMR Spectroscopy at High Field. *Angewandte Chemie International Edition* **2010**, *49*, 8657-8661.
42. Katada, N.; Nakata, S.; Kato, S.; Kanehashi, K.; Saito, K.; Niwa, M., Detection of Active Sites for Paraffin Cracking on USY Zeolite by ^{27}al MQMAS NMR Operated at High Magnetic Field 16 T. *Journal of Molecular Catalysis A: Chemical* **2005**, *236*, 239-245.
43. Kobera, L.; Brus, J.; Klein, P.; Dedecek, J.; Urbanova, M., Biaxial Q-Shearing of ^{27}Al 3QMAS NMR Spectra: Insight into the Structural Disorder of Framework Aluminosilicates. *Solid State Nuclear Magnetic Resonance* **2014**, *57–58*, 29-38.
44. Li, S.; Zheng, A.; Su, Y.; Zhang, H.; Chen, L.; Yang, J.; Ye, C.; Deng, F., Brønsted/Lewis Acid Synergy in Dealuminated HY Zeolite: A Combined Solid-State NMR and Theoretical Calculation Study. *Journal of the American Chemical Society* **2007**, *129*, 11161-11171.
45. Hu, J. Z.; Wan, C.; Vjunov, A.; Wang, M.; Zhao, Z.; Hu, M. Y.; Camaioni, D. M.; Lercher, J. A., ^{27}Al MAS NMR Studies of HBEA Zeolite at Low to High Magnetic Fields. *The Journal of Physical Chemistry C* **2017**, *121*, 12849-12854.
46. Neuhoff, P. S.; Zhao, P.; Stebbins, J. F., Effect of Extraframework Species on ^{17}O NMR Chemical Shifts in Zeolite A. *Microporous and Mesoporous Materials* **2002**, *55*, 239-251.
47. Yildirim, E. K. O-17 NMR Studies of Some Silicate Crystals and Glasses. The University of Warwick, Coventry, United Kingdom, 2000.
48. Lee, S. K.; Stebbins, J. F., Extent of Intermixing among Framework Units in Silicate Glasses and Melts. *Geochimica et Cosmochimica Acta* **2002**, *66*, 303-309.
49. Cheng, X.; Zhao, P.; Stebbins, J. F., Solid State NMR Study of Oxygen Site Exchange and Al-O-Al Site Concentration in Analcime. *American Mineralogist* **2000**, *85*, 1030.
50. Cong, X.; Kirkpatrick, R. J., ^{17}O Mas NMR Investigation of the Structure of Calcium Silicate Hydrate Gel. *Journal of the American Ceramic Society* **1996**, *79*, 1585-1592.
51. Zhao, P.; Neuhoff, P. S.; Stebbins, J. F., Comparison of FAM Mixing to Single-Pulse Mixing in ^{17}O 3Q- and 5Q-MAS NMR of Oxygen Sites in Zeolites. *Chemical Physics Letters* **2001**, *344*, 325-332.
52. Stebbins, J. F.; Lee, S. K.; Oglesby, J. V., Al-O-Al Oxygen Sites in Crystalline Aluminates and Aluminosilicate Glasses: High-Resolution Oxygen-17 NMR Results. *American Mineralogist* **1999**, *84*, 983.
53. Lee, S. K.; Stebbins, J. F., Al–O–Al and Si–O–Si Sites in Framework Aluminosilicate Glasses with Si/Al=1: Quantification of Framework Disorder. *Journal of Non-Crystalline Solids* **2000**, *270*, 260-264.
54. Loewenstein, W., The Distribution of Aluminum in the Tetrahedra of Silicates and Aluminates. *American Mineralogist* **1954**, *39*, 92-96.
55. Weng, L.; Sagoe-Crentsil, K., Dissolution Processes, Hydrolysis and Condensation Reactions During Geopolymer Synthesis: Part I—Low Si/Al Ratio Systems. *Journal of Materials Science* **2007**, *42*, 2997-3006.
56. Sagoe-Crentsil, K.; Weng, L., Dissolution Processes, Hydrolysis and Condensation Reactions During Geopolymer Synthesis: Part II. High Si/Al Ratio Systems. *Journal of Materials Science* **2006**, *42*, 3007-3014.

57. Davidovits, J. In *Properties of Geopolymer Cements*, First International Conference on Alkaline Cements and Concretes, Kiev, Ukraine, Scientific Research Institute on Binders and Materials: Kiev, Ukraine, 1994; pp 131-149.
58. Palomo, A.; Alonso, S.; Fernández-Jiménez, A., Alkaline Activation of Fly Ashes: NMR Study of the Reaction Products. *Journal of the American Ceramic Society* **2004**, *87*, 1141-1145.